Supplementary: Estimation of the Antarctic surface mass balance using MAR (1979-2015) and identification of dominant processes

Cécile Agosta[1,2,3], Charles Amory[1], Christoph Kittel[1], Anais Orsi[2], Vincent Favier[3], Hubert Gallée[3], Michiel R. van den Broeke[4], Jan T.M. Lenaerts[4,5], J. Melchior van Wessem[4], and Xavier Fettweis[1]

[1]F.R.S.-FNRS, Laboratory of Climatology, Department of Geography, University of Liège, B-4000 Liège, Belgium
[2]Laboratoire des Sciences du Climat et de l'Environnement (IPSL/CEA-CNRS-UVSQ UMR 8216), CEA Saclay, F-91190 Gif-sur-Yvette, France
[3]Université Grenoble Alpes, CNRS, Institut des Géosciences de lEnvironnement, F-38000, Grenoble,France
[4]Institute for Marine and Atmospheric Research Utrecht, Utrecht University, Utrecht, the Netherlands
[5]Department of Atmospheric and Oceanic Sciences, University of Colorado Boulder, Boulder CO, United States of America

April 11, 2018

Table S1: References of snow density datasets and number of observations/number of 35×35 km grid cells by depth range.

Reference	Dataset	0–20 cm	0–50 cm	0–100 cm
Albert et al. (2007)	SUMup17 [1]	3/1	3/1	3/1
Brucker and Koenig (2011)	SUMup17 [1]	6/5	6/5	6/5
Cameron et al. (1968)	Kaspers04 [2]	0/0	0/0	22/22
Ding et al. (2011)	CHINARE	568/39	0/0	0/0
Fujiwara and Endo (1971)	JARE69	65/38	0/0	13/13
Gallet et al. (2011)	DC-DDU08	8/8	7/7	0/0
Herron and Langway (1980)	Kaspers04 [2]	0/0	1/1	1/1
Kaspers et al. (2004)	Kaspers04 [2]	0/0	2/2	2/2
Kreutz et al. (2011)	SUMup17 [1]	1/1	1/1	1/1
Medley et al. (2013)	SUMup17 [1]	1/1	3/3	2/2
Sugiyama et al. (2012)	JASE07	0/0	43/43	43/42
Watanabe (1975)	JARE70	6/1	6/5	8/5
van den Broeke et al. (1999)	Kaspers04 [2]	0/0	8/8	8/8

[1] Montgomery et al. (2018), [2] Kaspers et al. (2004)

Table S2: Estimates of erosion-deposition fluxes summed over the total (TIS, 13.4 10^6 km^2) and the grounded (GIS, 12.0 10^6 km^2) Antarctic ice sheet, excluding Peninsula. Parenthesis (α_{max},ws_{min},ws_{max}) are for estimates of erosion-deposition based on a scaling of the curvature: erosion-deposition (kg m^{-2} yr^{-1}) = α (10^6 kg m^{-1} yr^{-1}) × curvature (10^{-6} m^{-1}), with $\alpha = 0$ (10^6 kg m^{-1} yr^{-1}) for wind speed lower than ws_{min} (m s^{-1}), $\alpha = \alpha_{max}$ (10^6 kg m^{-1} yr^{-1}) for wind speed greater than ws_{max} (m s^{-1}), and α linearly increasing as a function of wind speed in between. Wind speed is the annual average of 10 m wind speed of MAR forced by ERA-Interim.

Component	(3700,5,9)	(3700,6,8)	(4700,5,9)	(2700,5,9)	RACMO2
TIS w/o Peninsula					
Erosion (Gt yr^{-1})	82	81	95	66	21
Deposition (Gt yr^{-1})	74	74	88	58	16
Net (Gt yr^{-1})	8	7	7	8	5
GIS w/o Peninsula					
Erosion (Gt yr^{-1})	81	80	94	65	19
Deposition (Gt yr^{-1})	68	69	81	53	14
Net (Gt yr^{-1})	13	11	13	12	5

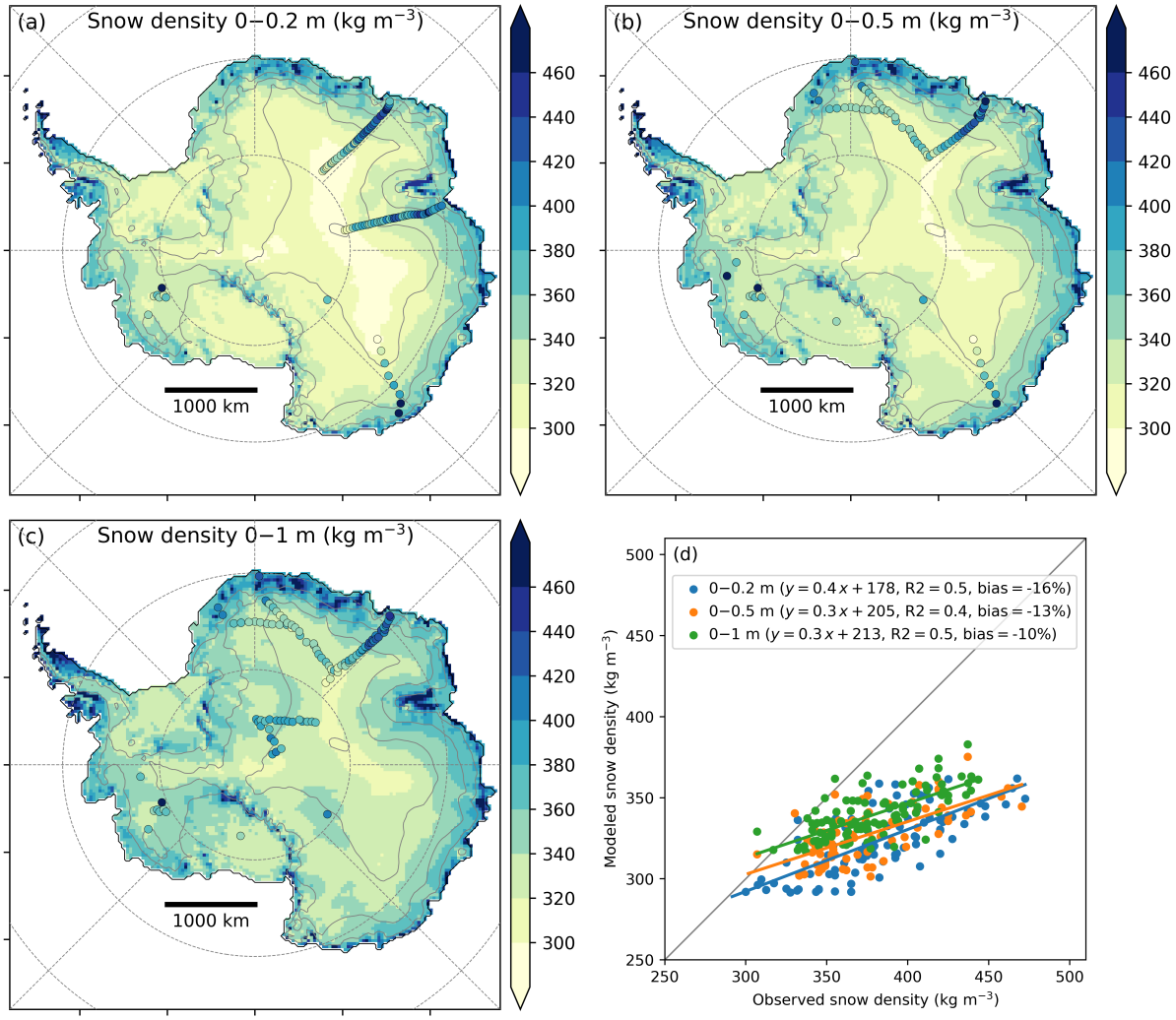

Figure S1: Snow density modelled by MAR (maps) and observations (dots) for (a) the first 20 cm of snow, (b) the first 50 cm of snow and (c) the first meter of snow, and (d) shows scatterplot of modelled versus observed snow density. The snow density database is detailed in Table S2. Modelled snow density is taken in average for the period 1979-2015. Observed snow density is averaged on MAR grid cells.

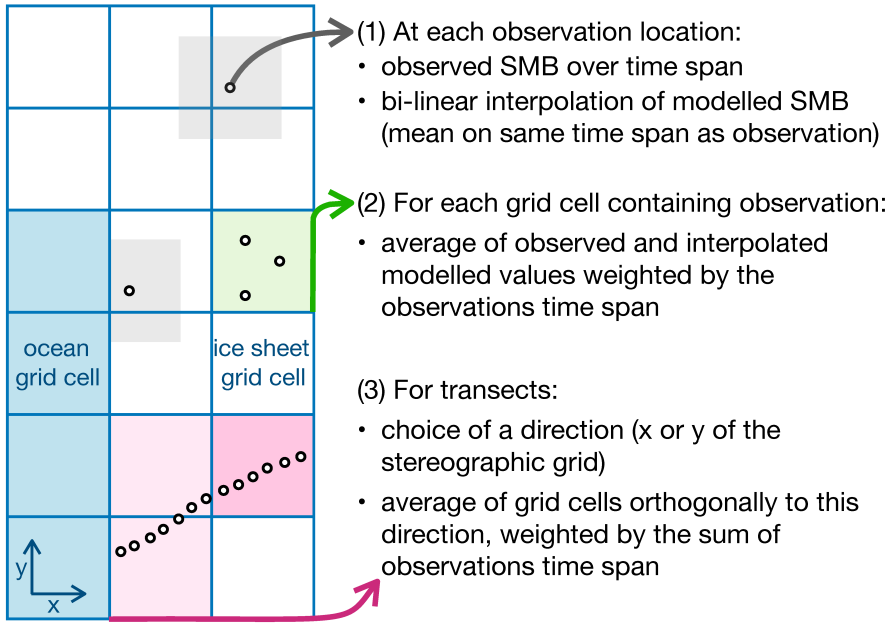

Figure S2: Sketch explaining the comparison method between observed (points) and modelled (gridded) SMB.

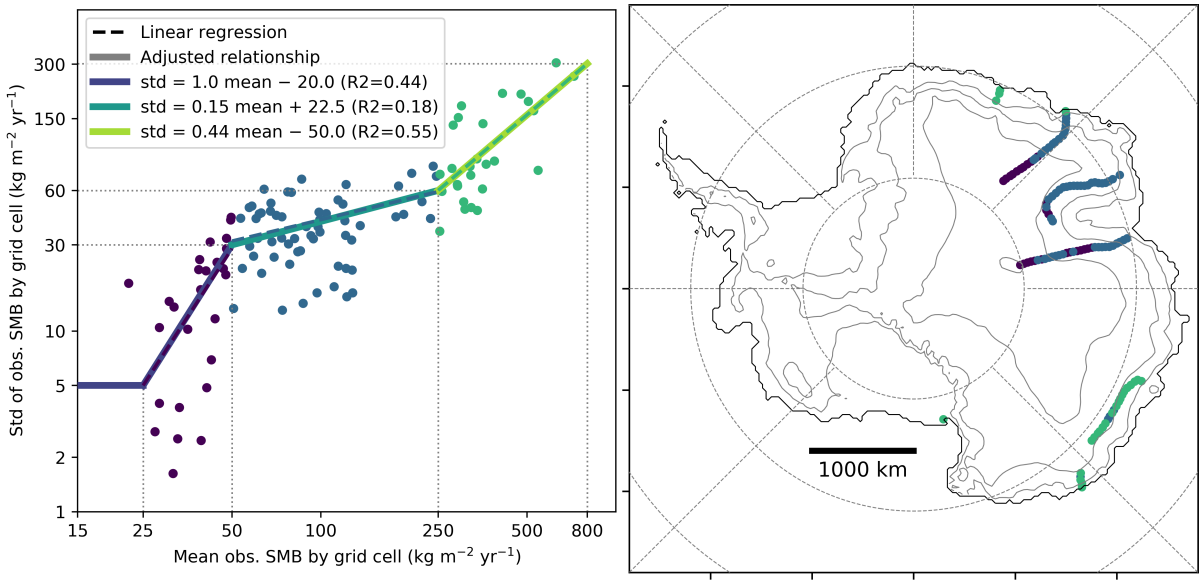

Figure S3: Estimate of the SMB spatial variability into 35 km×35 km grid cells as a function of mean observed SMB in the grid cell. (a) Standard deviation versus mean value of observed SMB for each MAR grid cell containing more than 10 observations. We delimitate three variability regimes depending on mean SMB values : <=50 kg m^{-2} yr^{-1}, [50-250] kg m^{-2} yr^{-1} and >=250 kg m^{-2} yr^{-1}. (b) Location of the SMB regimes, with same colour code as in panel (a).

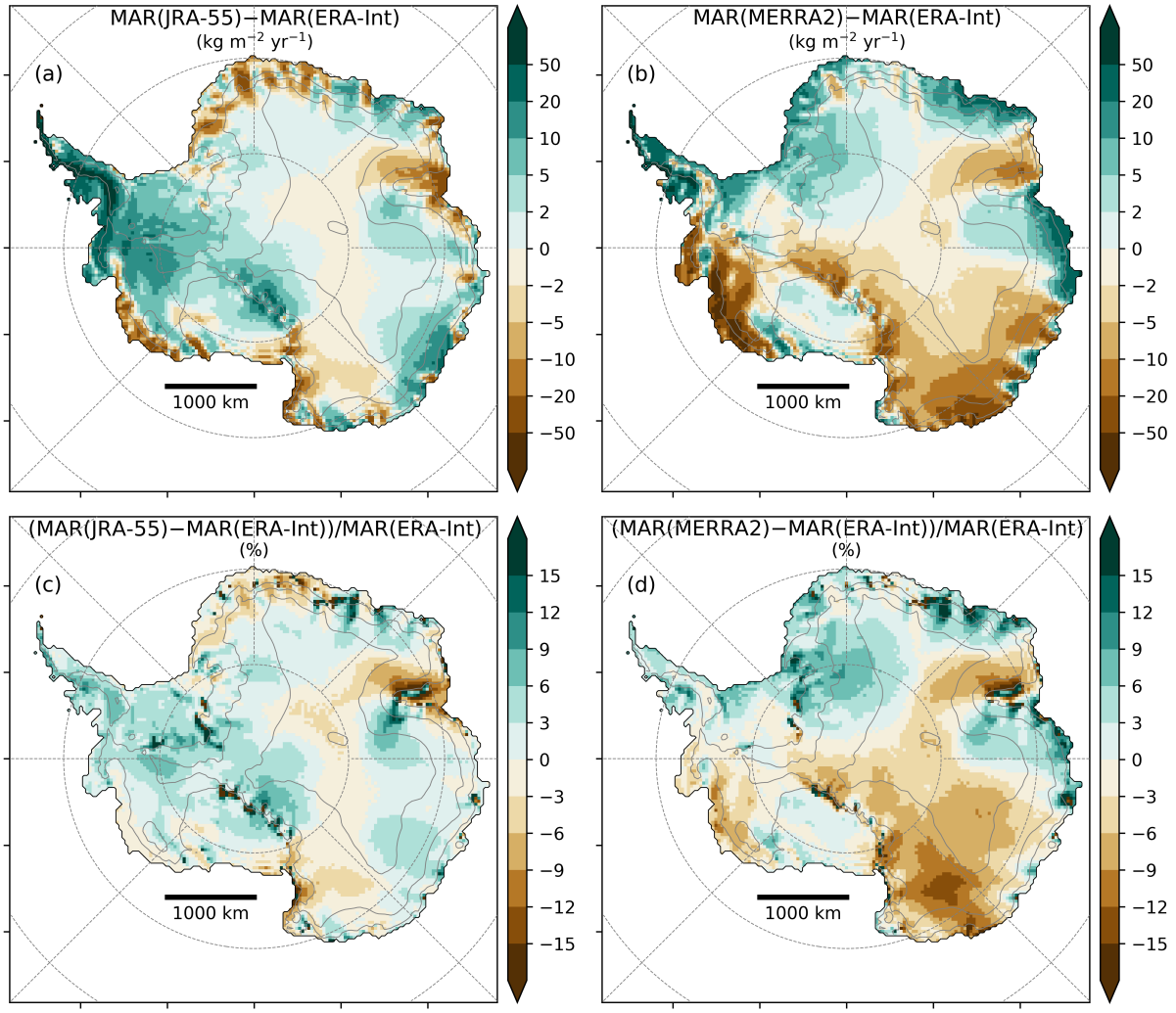

Figure S4: Difference between mean annual SMB modelled by MAR forced by (a) JRA-55 and (b) MERRA2 and MAR forced by ERA-Interim, for the period 1979-2015, in kg m^{-2} yr^{-1}. (c) and (d) are the same than (a) and (b) but divided by MAR(ERA-Interim) mean SMB (in %).

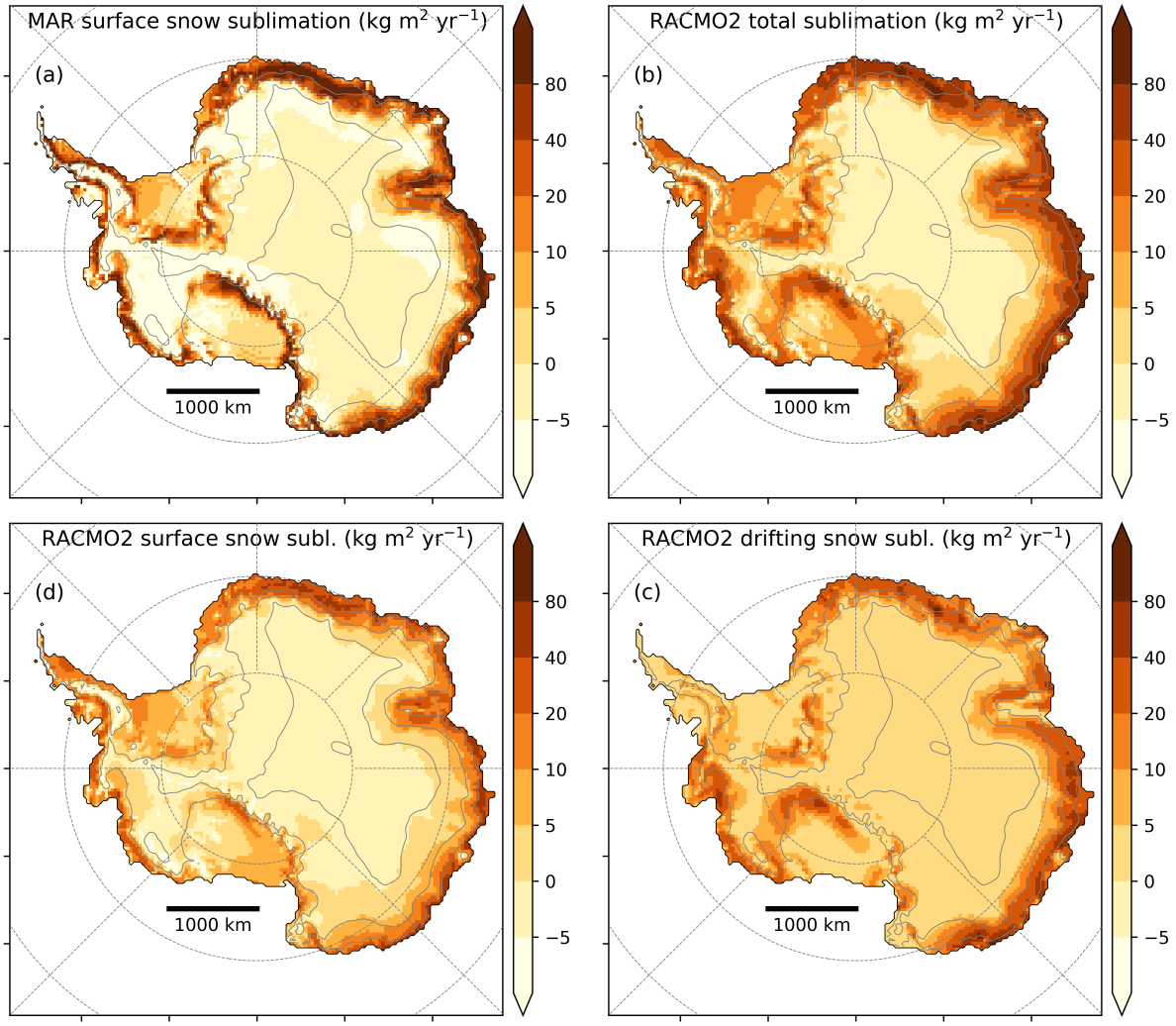

Figure S5: Annual mean modelled sublimation fluxes for the period 1979-2015, in kg m^{-2} yr^{-1}. (a) Sublimation at the surface of the snowpack modelled by MAR(ERA-Interim). (b) Total sublimation (surface snow sublimation plus drifting snow sublimation) modelled by RACMO2(ERA-Interim). (c) Same as (a) but for RACMO2(ERA-Interim). (d) Drifting snow sublimation modelled by RACMO2(ERA-Interim). MAR does not include drifting snow in these simulations.

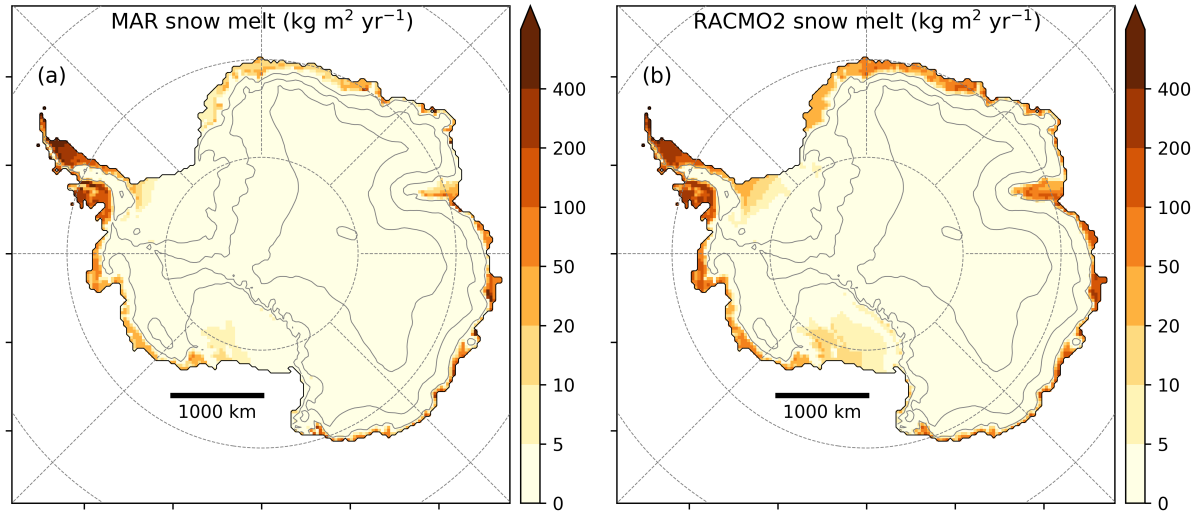

Figure S6: Snowmelt amounts modelled by MAR and RACMO2 forced by ERA-Interim for the period 1979-2015, in kg m^{-2} yr^{-1}. Note that snowmelt is almost totally refrozen in the snowpack in both models (Table 1).

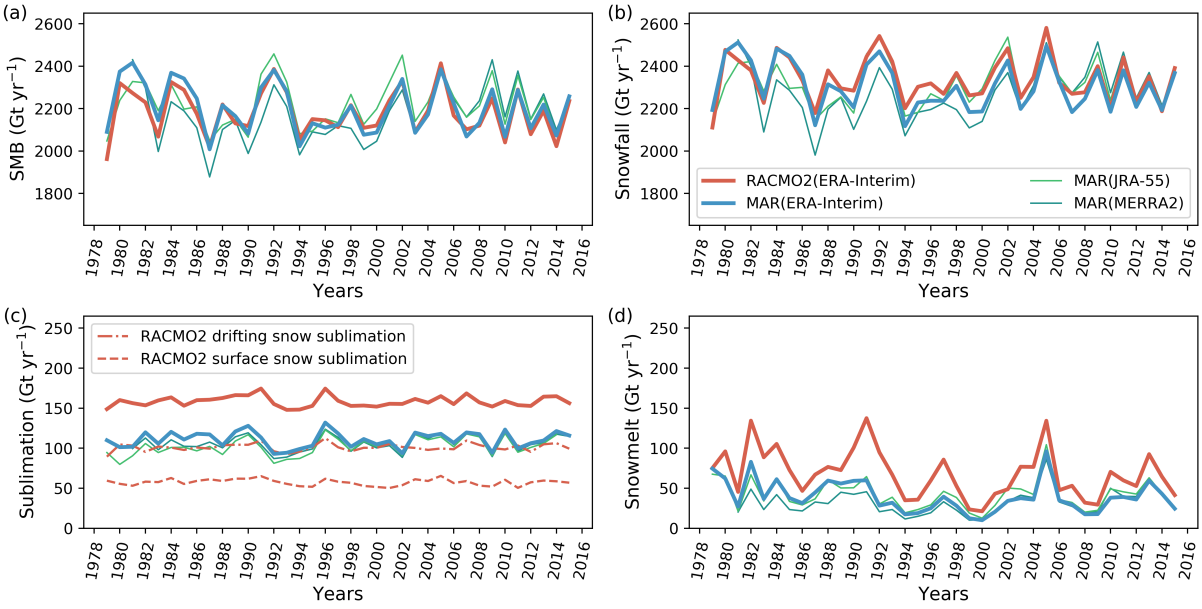

Figure S7: Annual SMB components summed over the Antarctic ice-sheet excluding peninsula (13.4 10^6 km^2), for (a) SMB, (b) snowfall, (c) sublimation and (d) snowmelt. Red solid thick line is for RACMO2(ERA-Interim), light green solid thin line is for MAR(ERA-Interim), blue solid thick line is for MAR(JRA-55) and dark green solid thin line is for MAR(MERRA2). Note that snowmelt is almost totally refrozen in the snowpack in both models (Table 1).

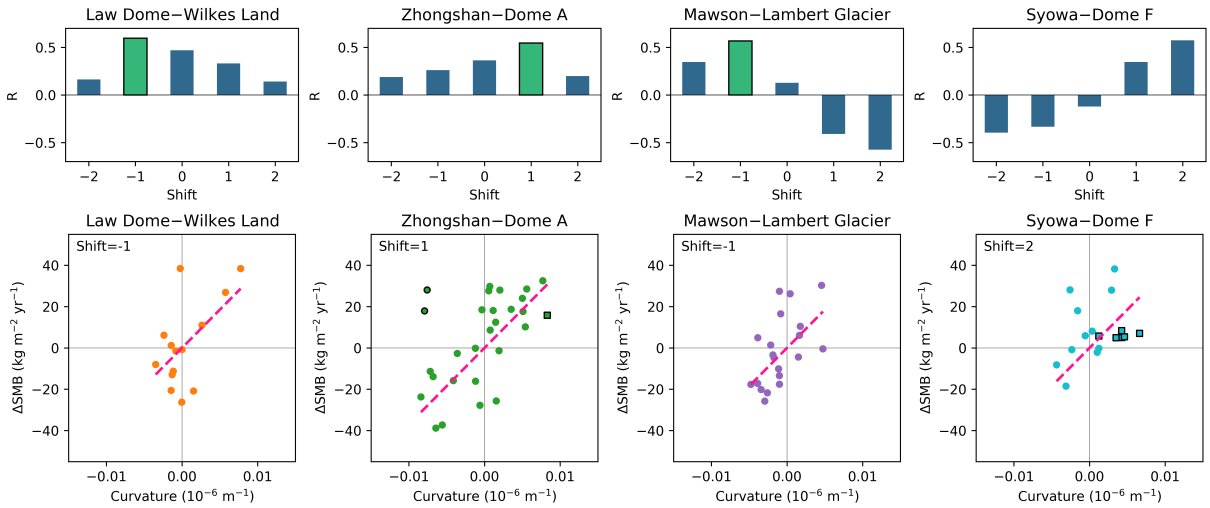

Figure S8: (top) Correlation coefficient R between MAR(ERA-Interim) SMB bias and curvature spatially shifted of -2, -1, 0, 1 and 2 grid cells. Green bars are for p-value lower than 0.05 and R greater than 0. (bottom) Scatterplots of MAR(ERA-Interim) SMB bias versus shifted curvature, with shift given at top left of each sub-figure. Pink dashed line is the regression line through origin computed for the four transects all-together (Fig. 4a). Dots and squares with black contour lines are excluded from regression. Squares are for locations where MAR annual 10 m wind speed in lower than seven m s^{-1}.

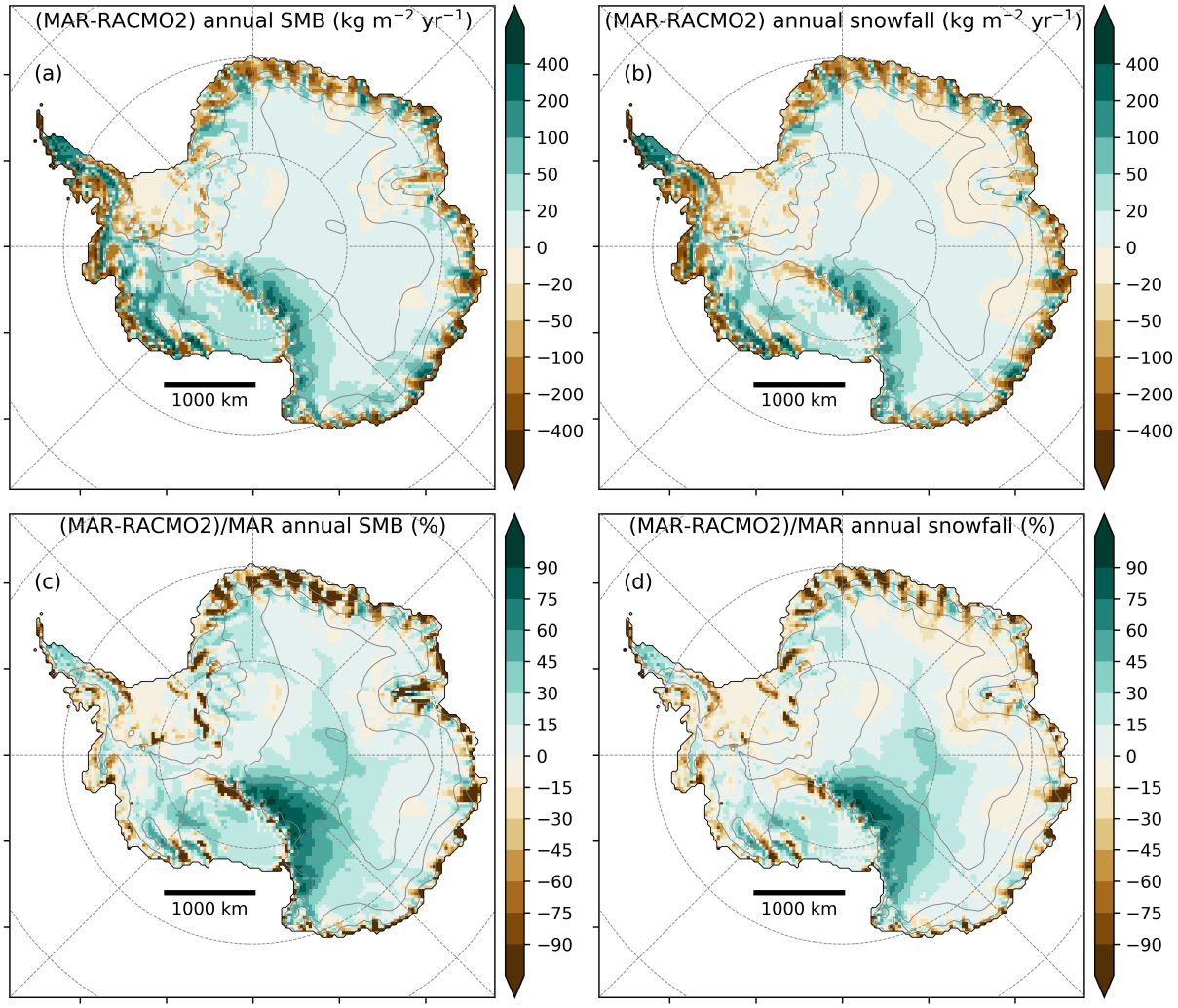

Figure S9: Difference between MAR and RACMO2 forced by ERA-Interim for the period 1979-2015 for (left) SMB (left) and (right) snowfall. (top) Absolute differences, in kg m^{-2} yr^{-1}, and (bottom) relative differences, in %.

References

Albert, M. R., Courville, Z., and Cathles, M.: Snow and Firn Permeability: Characteristics of Snow Megadunes and their Potential Effects on Ice Core Interpretation, U.S. ANTARCTIC PROGRAM DATA CENTER, https://doi.org/doi:10.7265/N5639MPD, URL http://www.usap-dc.org/view/dataset/609299, 2007.

Brucker, L. and Koenig, L.: Satellite-Era Accumulation Traverse 2011 (SEAT11) snowpit density data , Unpublished, 2011.

Cameron, R. L., Picciotto, E., Kane, H. S., and Gliozzi, J.: Glaciology of the Queen Maud Land Traverse, 1964-65 South Pole - Pole of Relative Inaccessibility, Research Foundation and the Institute of Polar Studies, The Ohio State University, 43212, URL http://hdl.handle.net/1811/38761, 1968.

Ding, M., Xiao, C., Li, Y., Ren, J., Hou, S., Jin, B., and Sun, B.: Spatial variability of surface mass balance along a traverse route from Zhongshan station to Dome A, Antarctica, Journal of Glaciology, 57, 658–666, https://doi.org/10.3189/002214311797409820, URL http://www.ingentaconnect.com/content/igsoc/jog/2011/00000057/00000204/art00008, 2011.

Fujiwara, K. and Endo, Y.: Report of the Japanese Traverse Syowa-South Pole 1968-1969, JARE Scientific Reports, pp. 68–109, 1971.

Gallet, J. C., Domine, F., Arnaud, L., Picard, G., and Savarino, J.: Vertical profile of the specific surface area and density of the snow at Dome C and on a transect to Dumont D'Urville, Antarctica – albedo calculations and comparison to remote sensing products, The Cryosphere, 5, 631–649, https://doi.org/10.5194/tc-5-631-2011, URL http://www.the-cryosphere.net/5/631/2011/, 2011.

Herron, M. M. and Langway, C. C.: Firn Densification: An Empirical Model, Journal of Glaciology, 25, 373–385, https://doi.org/10.3189/S0022143000015239, URL https://www.cambridge.org/core/product/identifier/S0022143000015239/type/journal_article, 1980.

Kaspers, K. A., van de Wal, R. S., van den Broeke, M. R., Schwander, J., Van Lipzig, N. P. M., and Brenninkmeijer, C. A. M.: Model calculations of the age of firn air across the Antarctic continent, Atmospheric Chemistry and Physics, 4, 1365–1380, URL http://atmos-chem-phys.net/4/1365/2004/acp-4-1365-2004.pdf, 2004.

Kreutz, K., Koffman, B., Breton, D., and Hamilton, G.: Microparticle, Conductivity, and Density Measurements from the WAIS Divide Deep Ice Core, Antarctica, U.S. ANTARCTIC PROGRAM DATA CENTER, https://doi.org/10.7265/N5K07264, URL http://www.usap-dc.org/view/dataset/609499, 2011.

Medley, B., Joughin, I., Das, S. B., Steig, E. J., Conway, H., Gogineni, S., Criscitiello, A. S., McConnell, J. R., Smith, B. E., van den Broeke, M. R., Lenaerts, J. T., Bromwich, D. H., and Nicolas, J. P.: Airborne-radar and ice-core observations of annual snow accumulation over Thwaites Glacier, West Antarctica confirm the spatiotemporal variability of global and regional atmospheric models, Geophysical Research Letters, 40, 3649–3654, https://doi.org/10.1002/grl.50706, URL http://onlinelibrary.wiley.com/doi/10.1002/grl.50706/full, 2013.

Montgomery, L., Koenig, L., and Alexander, P.: The SUMup Dataset: Compiled measurements of surface mass balance components over ice sheets and sea ice with preliminary analysis over Greenland, Earth System Science Data Discussions, pp. 1–31, https://doi.org/10.5194/essd-2018-21, URL https://www.earth-syst-sci-data-discuss.net/essd-2018-21/, 2018.

Sugiyama, S., Enomoto, H., Fujita, S., Fukui, K., Nakazawa, F., Holmlund, P., and Surdyk, S.: Snow density along the route traversed by the Japanese–Swedish Antarctic Expedition 2007/08, Journal of Glaciology, 58, 529–539, URL http://www.ingentaconnect.com/content/igsoc/jog/2012/00000058/00000209/art00008, 2012.

van den Broeke, M. R., Winther, J.-G., Isaksson, E., Pinglot, J. F., Karlof, L., Eiken, T., and Conrads, L.: Climate variables along a traverse line in Dronning Maud Land, East Antarctica, Journal of Glaciology, 45, 295–302, https://doi.org/10.3189/S0022143000001799, URL https://www.cambridge.org/core/product/identifier/S0022143000001799/type/journal_article, 1999.

Watanabe, O.: Density and hardness of snow in Mizuho Plateau-West Enderby Land in 1970–1971, JARE Data Reports, 27, 187–235, 1975.